applied optics

Simulation on antireflection of the oxide nanosphere monolayer film

Yuxiao Hou,[1] Xiaohong Li,[1,3] Hang Luo,[1] Wei Lei,[1] and Hong Lei[2,4]

[1]School of Science, Southwest University of Science and Technology, Mianyang 621010, China
[2]State Key Laboratory for Environment-friendly Energy Materials, Southwest University of Science and Technology, Mianyang 621010, China
[3]e-mail: lixiaohong@swust.edu.cn
[4]e-mail: honglei@swust.edu.cn

Received 18 March 2019; revised 24 May 2019; accepted 28 May 2019; posted 28 May 2019 (Doc. ID 362613); published 13 June 2019

We theoretically simulate the antireflective effects of oxide nanosphere monolayer films in the visible spectrum. The essential geometric and material parameters of nanosphere films are simulated and different functions are proposed to describe the dependence of reflectance on the influencing factors. The rational function is fitted to describe the monotonic decreasing of reflectance on the ratio of nanospheres' radius to incident wavelength. At a wavelength of 550 nm and incidence at 75°, the reflectance of the glass substrate coated with SiO_2 decreases to 14.1% compared with 41.7% of the uncoated glass. The results have an excellent potential for applications in optical devices such as filters, polarizing elements, and camera lenses.

https://doi.org/10.1364/AO.58.004926

1. INTRODUCTION

In recent years, there has been a breakthrough in the development of antireflection due to the strong desire to improve the performance of optical and optoelectronic components, such as lenses, solar cells, and high digital screens. Currently, antireflection methods can be divided into dielectric interference coatings, surface texturing, adiabatic index matching, and scattering from plasmonic nanoparticles [1]. By removing the mismatch impedance between the heterogeneous media at the interface [2], the antireflection technology eliminates unwanted light loss, thereby increasing the incident efficiency. With the development trend of component integration and miniaturization, the sub-wavelength structures have received extensive attention [3–6] in the antireflection effect. With many tunable factors, such as the period, depth and cross-sectional geometry, now the sub-wavelength structures have turned into many mature shapes [7–10]. Among them, nanospheres [11] have self-assembly ability and are not affected by the optical diffraction limit in the preparation process [12]. Compared with the preparation of sub-wavelength nanostructures by deep ultraviolet exposure or electron beam exposure [12], the oxide nanosphere film has lower cost, more conventional structure, shorter productive period, and more controllable antireflection in the visible light. Then a question comes out whether a monolayer film of nanospheres could also lead to a striking antireflection effect. The answer has proved to be yes [13]. Not only that, the single-layer nanosphere film can be coated on both sides of the glass [14] and work in 300–1300 nm [15]. Compared to the bulk film mostly used in single wavelength, the monolayer nanosphere film performs a more extensive antireflection effect with large angle and wide spectrum. Furthermore, by combining the radius, concentration, and type of nanospheres, a single-layer nanosphere film can even have more functions like self-cleaning capacity [16], super-hydrophilicity [17], hydrophobicity [18], and antifogging property [19]. However, the dependence of reflectance on geometric and material parameters of nanosphere antireflection films is very complicated and there is a lack of related work. Our work is a combination of the influential factors for the monolayer nanosphere film. The results not only further verify the antireflective effect of the monolayer nanosphere film but also provide deep understandings for the corresponding studies by quantitative functions.

In this work, we mainly focus on the reflectance law of oxide nanosphere monolayer film under large incident angle and systematically summarize the antireflective laws of oxide nanosphere film from a theoretical perspective. We simulate the appearance of the film surface by building a three-dimensional periodic model. In most cases, the general evolution of optical properties with geometric and material parameters are not entirely taken into account [20]. Motivated by a simulation with different glass substrates [21], we intend to combine and quantify the influential factors by functions, including nanosphere radius (r), incident wavelength (λ), polarization state (s), relative refractive index difference (Δ), and surface roughness (D). Inspired by the previous experiments [13,14], our simulation has enough reliability and flexibility because of its simply changed parameters and extensive ranges. This study can simplify the nanosphere film fabrication experiments and is readily applicable to various fields, especially in transparent optics like filters, polarizing elements, and camera lenses.

2. MODELING

This simulation uses the wave optics module of COMSOL Multiphysics. To simulate the refractive interface formed by the nanospheres and the substrate, we have established a three-dimensional cube with size $\lambda \times \lambda \times 2\lambda$ as one periodic unit model, as shown in Fig. 1(a). The model can be divided into three parts according to the refractive index: air ($n_A = 1$), nanosphere layer ($n_N = 1.40$–2.35) [22], and glass substrate ($n_B = 1.5$). Among the oxide nanospheres, SiO_2($n_s = 1.45$) has low cost and stable chemical properties and has been widely used in optical coatings, sensors, and other fields [23]. Therefore, we choose SiO_2 nanospheres as the principal research object. Larger nanospheres bring rougher surface and more scattering; therefore, we only demonstrate the results of oxide nanospheres with a radius from 10 to 80 nm, making sure $r/\lambda \ll 1$ for visible light.

The unit cell composes of two kinds of depression: uniform and random [Figs. 1(b) and 1(c)]. When all the nanospheres are uniformly depressed, the distance between nearest neighboring nanospheres is equal to λ, which means they are densely packed. Moreover, the sample step of each depression is $5\% \times r$. Ideally, the film is entirely uniform depressed, as shown in Fig. 1(b); wherein, the uniform depression refers to the surface simultaneous lower depth D. However, due to the unavoidable factors in fabrication techniques [1], the film has inevitable random depressions, as shown in Fig. 1(c), where we set each nanosphere depressed at a fluctuating depth of $5\% \times r$ around the uniform depression. The randomness of 5% of the radius is a critical value because the randomness below 5% is enough to display different types of the substrate surface and will not disturb the next depression sample. When all the nanospheres are uniformly recessed by 5% of the radius, the random depressed nanosphere can have any depth in 0%–10% (excluded) of the radius, as shown in Fig. 1(c), but the average depths of the uniform and random depression are the same.

The incident light is loaded by port by the upper surfaces of the model and incidents in the XOY plane along the angle θ with the z-direction, varying from 0° to 90°. R is the total reflectance of the nanosphere film. The nanosphere film conforms to the Floquet periodic condition and the wave vector for the Floquet periodicity is calculated by periodic ports. Tetrahedral meshes are selected in this model. The maximal mesh element size is 28 nm and the minimal is 1 nm. Even though the meshes are divided finer, the results of the solutions are left unchanged and the convergence of our simulation results has been verified.

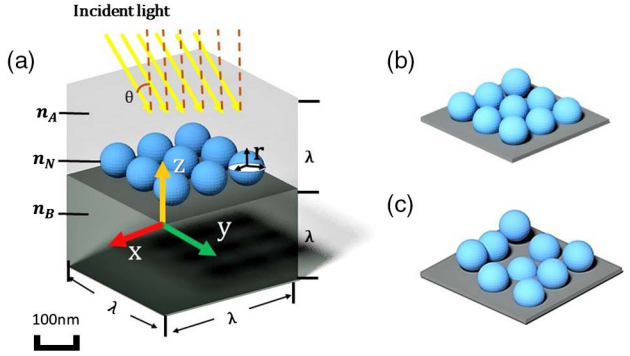

Fig. 1. (a) Model of the nanosphere coating film. (b) Uniform depression on the surface of the nanosphere film. (c) Random depression on the surface of the nanosphere film.

The wave equations in the frequency domain for the wave optics module of COMSOL Multiphysics are given as

$$\nabla \times (\mu_r^{-1} \nabla \times \mathbf{E}) - k_0^2 \left(\varepsilon_r - \frac{i\sigma}{\omega \varepsilon_r} \right) \mathbf{E} = 0, \tag{1}$$

where $\mathbf{E}$ is the electric and magnetic field amplitudes, μ_r and ε_r are respectively the relative permeability and permittivity of the medium, k_0 is the wave vector, and σ is the conductivity.

Usually, the traditional method for reflectance problems is to perform an effective approximation of the refractive index based on the Maxwell–Garnett theory. At the sub-wavelength scale, we also perform a comparison between the effective refractive index and our simulation to figure out whether a difference exists. Under wave propagation, we can consider that an inhomogeneous film is composed by many layers of "homogeneous" mixtures. Thus, the effective refractive index can be determined as a whole. Based on the Maxwell–Garnett model [24], the effective refractive index n can also be evaluated from the equation

$$\left[\frac{n^2 - n_1^2}{n^2 + 2n_1^2} \right]^2 = (1 - f) \left[\frac{n_2^2 - n_1^2}{n_2^2 + 2n_1^2} \right]^2, \tag{2}$$

where n_1 and n_2 are the refractive indices of media and f is the volume fraction of the medium. When the surface roughness is reduced to the sub-wavelength scale, the axially varying effective refractive index can provide a smoother graded transition of refractive index between air and the substrate. Consequently, the undesirable reflectance will be eliminated by infinitely approximating the continuous changes in the refractive index of an interface.

3. RESULTS

The radius of the nanosphere is the core factor affecting the antireflection effect of the nanosphere film [25]. Figures 2(a) and 2(b) show the effects of 10–80 nm SiO_2 nanospheres for an incident angle between 0° and 90°. The incident light wavelength is chosen as 550 nm because it is the key choice for spectral line calibration. The polarization state of the system is $s{:}p = 1{:}1$. According to Fig. 2(a), when $\theta \leq 45°$, the reflectance only increases by 1%–4.5%. So we focus on $\theta > 45°$, shown in Fig. 2(b). When the 550 nm light is incident at 75°, the reflectance of the 10–80 nm SiO_2 nanosphere film ranges from 14.1%–25.3% compared to 41.7% on ordinary uncoated glass. It means that the nanosphere film can relatively cut down the reflectance at least by 39.5%–66.3% with a large-angle incidence. We calculated the reflectance of the uncoated glass both by the Fresnel equation and simulation with the same incident condition ($\lambda = 550$ nm, $\theta = 75°$) and the two results are the same. To better characterize the wavelength's effect on the reflection, we plotted Figs. 2(c) and 2(d). Figures 2(c) and 2(d) show the wavelength's effect on the reflectance when $45° \leq \theta \leq 90°$. Figure 2(d) is the two-dimensional show of Fig. 2(c). When the radius is known, the reflectance ranges during 8%–25% at the short wavelength and 19%–25% in the long wavelength. The longer wavelength

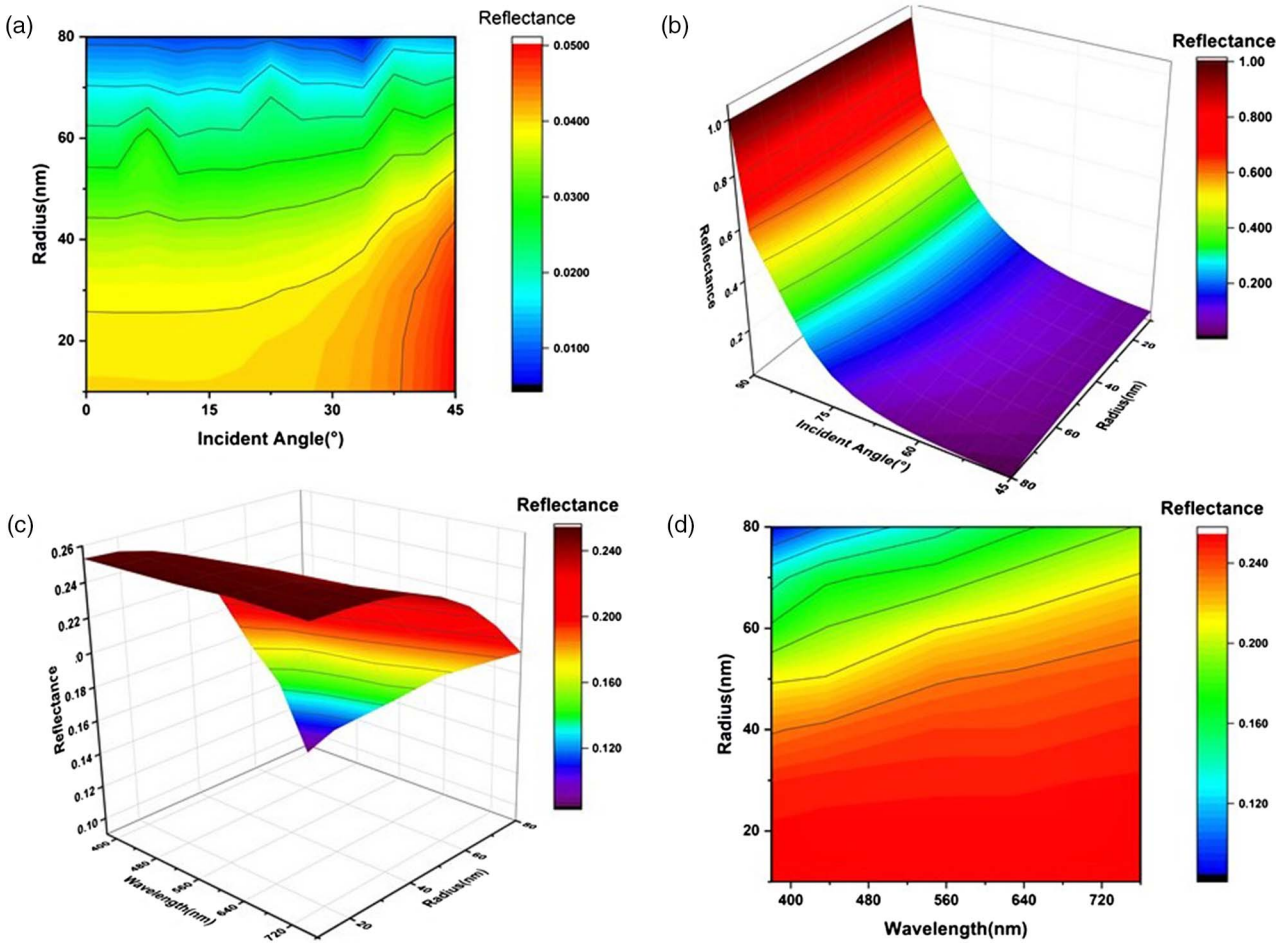

Fig. 2. Effects of radius and wavelength on reflectance. (a) Nanosphere radius's effect on the reflectance when $\theta = 0°$–$45°$. (b) Nanosphere radius's effect on the reflectance when $\theta = 45°$–$90°$. (c),(d) Wavelength's effect on the reflectance when $\theta = 45°$–$90°$.

brings higher reflectance. The ratio of the nanospheres' radius to the wavelength is an important parameter. When $r \ll \lambda$, the interface becomes a discontinuous boundary [3,5,6,8]. When r/λ becomes larger, the boundary tends to be continuous, which means the graded refractive index of the film becomes smoother, resulting in the stronger antireflective effect. So, to realize a better antireflection effect in the wide spectrum, we can use a larger radius (but still in the sub-wavelength) of nanospheres.

Polarization is an essential physical property of light. Differently polarized light leads to different surface reflection according to Fresnel equations. When $\theta = 0°$ or $90°$, s and p polarization show the same reflectance, while when $\theta = 0° - 90°$, s and p polarization have different reflectance trends. This effect of polarization on the reflection will help to decline the glare in particular directions. Also, materials have an essential physical property, the refractive index, which can affect the light's propagation and film's antireflection effect. In

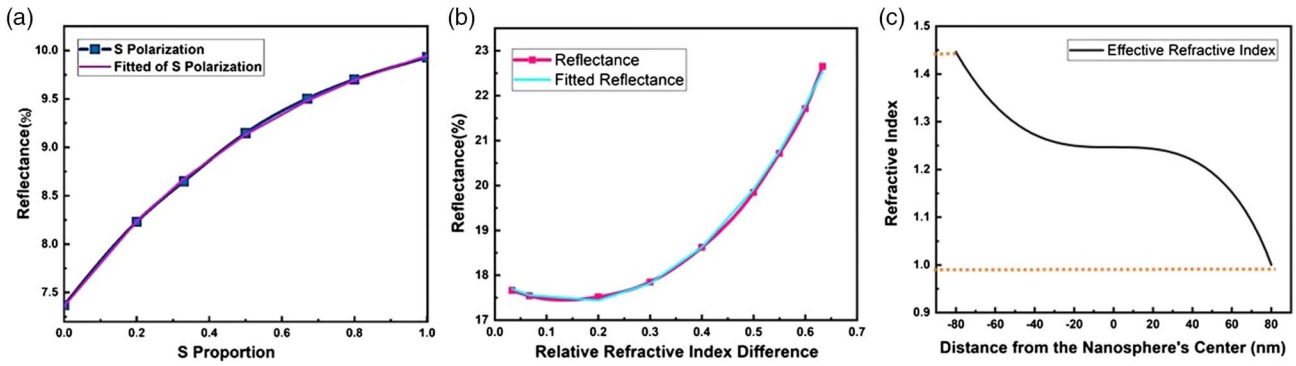

Fig. 3. Polarization and materials effect on the reflectance. (a) S-polarized proportions effect on reflectance. (b) Relationship between relative refractive index difference and reflectance. (c) Distribution of effective refractive index in the z-direction with 80 nm nanosphere.

Table 1. Reference for Nanosphere Materials [26,27]

Material	Refractive Index	Minimum Radius (nm)
SiO_2	1.45	7
Al_2O_3	1.63	20
MgO	1.70	50
ZnO	2.00	10
TiO_2	2.35	5

Fig. 3, we simulated the polarization and materials' effect on the reflectance when $r = 70$ nm and $\lambda = 550$ nm. In Fig. 3(a) we studied the trend of the surface reflectance with the proportion of the *s*-polarized state in the incident light. The ratio s of *s*-polarized light in the incident light takes from 0% to 100%. We can see that the influence of the polarization state on reflectance is within 3%, and the trend of change is similar to the exponential change. In Fig. 3(b), we use the relative refractive index difference $\Delta = (n_B - n_N)/n_B$ to describe the contribution of materials to reflectance. It can accommodate different nanospheres and substrate materials. According to the common nanosphere materials on the market, the relative refractive index difference $\Delta = 0.03$–0.63 for some typical oxides with $r = 10$–80 nm is shown in Table 1.

In Fig. 3(b), under the same stimulated environment, the relative refractive index difference makes the reflectance above 17%. As the difference in refractive index between the film material and the substrate increases, the absolute reflectance change fluctuates around 6%.

Another alternative way to describe the optical properties of nanosphere interface is the effective refraction index. When the nanospheres are uniformly distributed on the film's surface, through Eq. (2), we gradually calculate the effective refractive index of the film from the substrate to the air, shown in Fig. 3(c). Through weighting the area of Fig. 3(c), the average equivalent refractive index is 1.24. With a similar reflectance changing tendency, when $\theta \leq 30°$, the results from our simulation and the effective refractive index can be replaced by each other because $\eta \leq 2\%$; here η is the relative error between the refractive index approximation and the simulation. When $\theta \geq 45°$, $\eta \geq 10\%$. Therefore, the antireflection effect under large angle incidence at the sub-wavelength scale cannot be precisely calculated by the effective refractive index.

The depression degree of the nanospheres reflects the surface roughness, which is another critical factor influencing the reflective properties of the film surface. Figure 4 shows the effects of

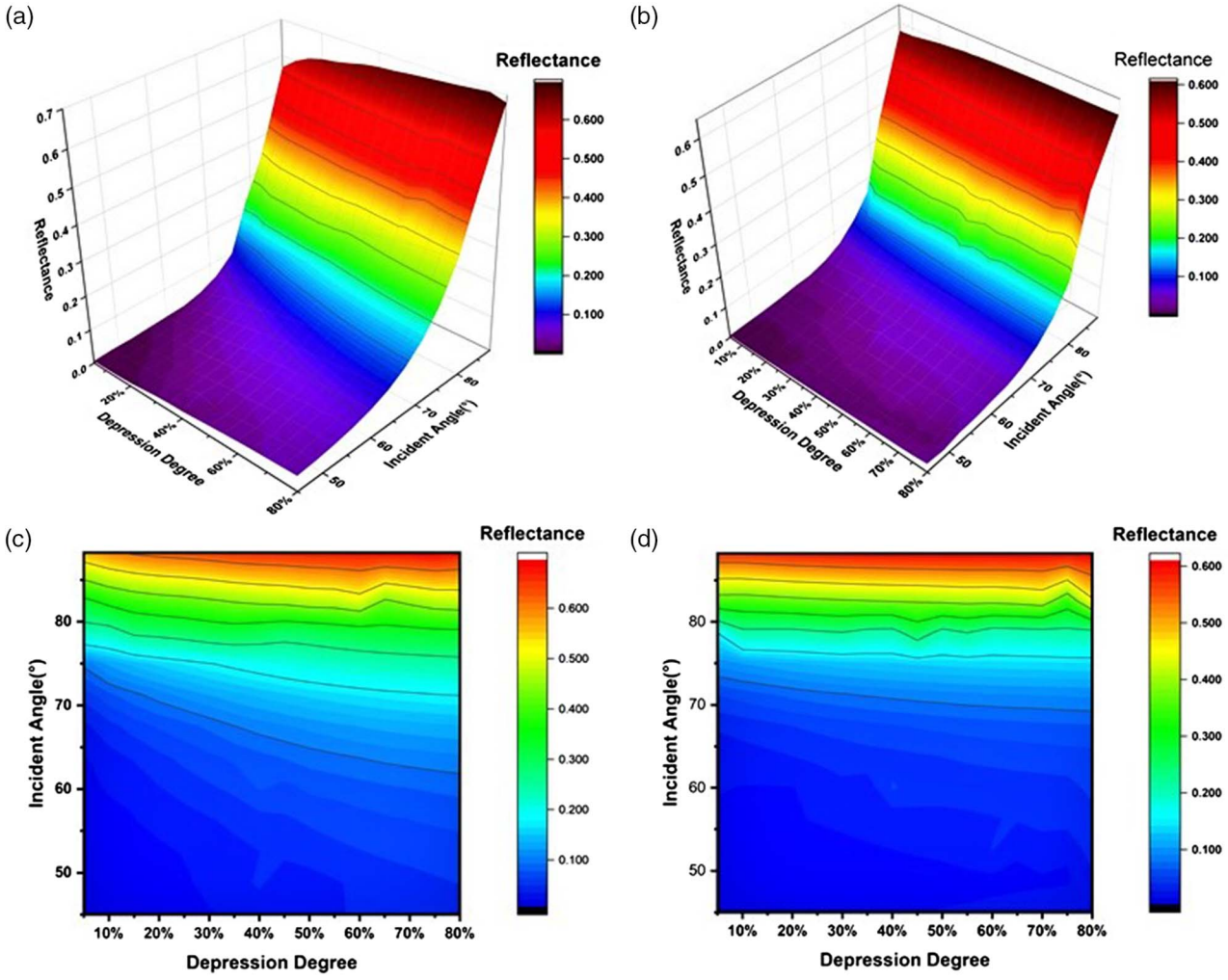

Fig. 4. Effects of the surface depressions' degree and uniformity. (a),(c) Uniform depression's effect on the reflectance. (b),(d) Random depression's effect on the reflectance. (c) Reflectance distribution of (a) in two dimension. (d) Reflectance distribution of (b) in two dimension.

the surface depressions' degree and uniformity when $\theta \geq 75°$. The comparison of Figs. 4(a) and 4(b) reveals that the impact of uniform depression and random depression on reflectance is similar. However, according to Figs. 4(c) and 4(d), the surface reflectance of the uniform depression is twice as large as the random depression at the incidence of 75°. Under the same simulation conditions, the depression's randomness has an influence limited to 2% on reflectance. Although both of the uniform and random depressions have a similar influence on the reflectance because their average depths are the same throughout the simulation, compared with the uniform depression, the random depressed nanospheres relatively deepen the gaps between nanospheres and induce less reflectance than that of the uniform depression under the same simulating condition.

4. DISCUSSION

To further analyze the influential factors of nanosphere film reflectance, we fit the geometric and material parameters of nanosphere films relating to reflectance under different incident conditions, shown in Figs. 3(a) and 3(b) and Figs. 5(a) and 5(c). First, let us discuss the nanosphere radius because it is the most critical factor affecting the reflectance of the film. Second, we explore how λ, s, Δ, and D affect the total reflectance R under the known nanosphere radius ($r = 70$ nm). In Fig. 5(a), we have shown that the nanosphere's radius has a consistent effect on antireflection when $0° \leq \theta \leq 90°$. Therefore, in Figs. 5(b) and 5(c) and Figs. 3(a) and 3(b) we mainly discuss the law at 75° to show the regularity more obviously.

According to the simulation results of Fig. 5(a) that the reflectance decreases with the radius of nanospheres changing from 10 to 80 nm, the reflectance dependence on the nanosphere radius satisfies rational function as

$$R\left(\frac{r}{\lambda}\right) = \frac{a_1 + a_2 \times \frac{r}{\lambda}}{1 + a_3 \times \frac{r}{\lambda} + a_4 \times \left(\frac{r}{\lambda}\right)^2}, \tag{3}$$

where R is still the total reflectance; r/λ is the normalization for radius r by incident wavelength λ. $a_{i(i=1,2,3,4)}$ are the dimensionless parameters describing $R(r)$, which change with λ, s, Δ, and D. When $r/\lambda \to \infty$, $R \to 0$. Since the nanosphere film is a single layer, when $r \to \infty$, it means that the film roughness

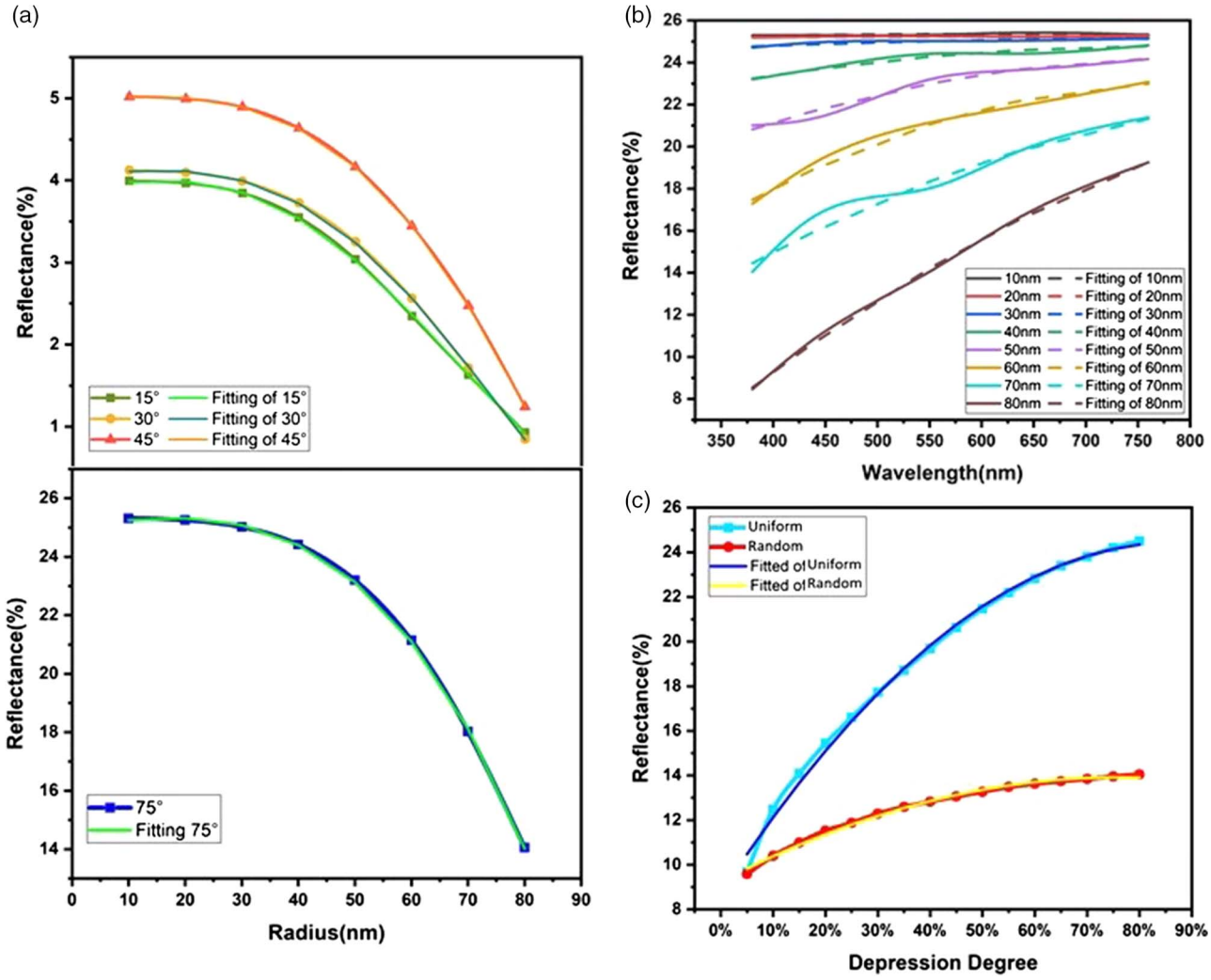

Fig. 5. Fittings of the results. (a) Radius effect on reflectance with incident angle $\theta = 15°$, 30°, 45°, and 75°. (b) Wavelengths' effect on reflectance. (c) Reflectance comparison between uniform and random depression. Both (b) and (c) are under 75° incidence. All incidence with polarization state $s{:}p = 1{:}1$.

Table 2. Relationship Between λ, s, Δ, D, and a_i

λ (nm)	S:P	Δ	D	$a_1(10^{-1})$	$a_2(10^{-3})$	$a_3(10^{-2})$	$a_4(\times 10^{-5})$
550	1:1	0.033	5% × r	2.495 ± 0.012	−2.410 ± 0.049	−1.118 ± 0.015	4.662 ± 0.427
550	1:2	0.033	5% × r	2.913 ± 0.021	−3.035 ± 0.064	−1.310 ± 0.010	8.060 ± 0.144
550	1:1	0.33	5% × r	3.043 ± 0.018	−3.072 ± 0.025	−1.157 ± 0.015	4.267 ± 0.097
550	1:1	0.033	50% × r	2.501 ± 0.016	−1.224 ± 0.022	−0.572 ± 0.013	2.613 ± 0.238
630	1:1	0.033	5% × r	2.525 ± 0.015	−2.289 ± 0.086	−1.014 ± 0.016	3.008 ± 0.541

is infinite. This is just like beams of sunlight being incident in an extremely lush jungle. Therefore, there is no reflection of the system. Moreover, when $r \to 0$, $R \to a_1$, that is $R(0) = a_1$, which means a_1 is the surface reflection produced by the substrate itself. When the radius of the nanosphere ranges 50–80 nm, R is relatively affected by 2%–3%. When adjusting λ, s, Δ, and D for different conditions, the parameters corresponding to a_1, a_2, a_3, and a_4 in Eq. (3) are given in Table 2; here the confidence limit of a_i is 95%. Comparing these values, we find that a_1 and a_4 are always positive, and a_1 is 4 orders of magnitude larger than a_4. Also, a_2 and a_3 are both negative and a_2 is an order of magnitude smaller than a_3. After simulations with a larger radius [28], this formula can be developed for the antireflection film with oxide spheres from a nanosize to microsize level. According to Table 1, since the value of $a_4 \times (r/\lambda)^2$ is quite small, we simplify Eq. (3) by eliminating the parameter a_4, shown in Eq. (4):

$$R\left(\frac{r}{\lambda}\right) = \frac{a_1 + a_2 \times \frac{r}{\lambda}}{1 + a_3 \times \frac{r}{\lambda}}. \tag{4}$$

Deviations from the data shown in Fig. 5(b) and a rational function [Eq. (4)] are originally from the model's simplification and ideality.

Based on Fig. 3(a), when specifying $s = 0\%$–100%, the corresponding reflectance increases with the s-polarized light. When $s = 0$, the p-polarization state takes a full responsibility. The fitting function for the polarization's effect is exponential and written as

$$R(s) = R_1 + b_1 e^{-b_2 s}. \tag{5}$$

Just like Eq. (3), R_1 is also an initial value. b_1 and b_2 include the influences of r, s, Δ, D, and θ. When $r = 70$ nm, $\lambda = 550$ nm and $s = 0\%$–100%, the reflectance of the nanosphere film fluctuates by 3%.

We use relative refractive index difference Δ to show the nanosphere materials' effect on the reflectance, as Fig. 3(b). It is monotonically increasing like the effect of the polarization state, but the curvature changing is opposite. The fitting quadratic function $R(\Delta)$ shows the relationship between the reflectance and relative refractive index difference Δ and is written as

$$R(\Delta) = R_2 + c_1 \times \Delta + c_2 \times \Delta^2. \tag{6}$$

The factors c_1, c_2 are comprehensively determined by the other parameters. When $r = 70$ nm, $\lambda = 550$ nm and $s = 50\%$, for the alternative oxide, the relative refractive index difference has 5% influence on the reflectance. Furthermore, under the same incident conditions, when the size of the nanospheres is smaller than 40 nm, the change in reflectance can be ignored.

The depression of the nanospheres is another crucial factor affecting the reflectance. When $r = 70$ nm, $\lambda = 550$ nm, we set a synchronous depression. This means that all the nanospheres in the unit cell have recessed to the same extent d, then the depression depth is $D = d \times r$. Meanwhile, for a random depression, we introduce the randomness into D. With a same average depression depth, we compare the influences of the depression uniformity. According to the numerical calculation, the effects of both the uniform and random depressions show the exponential distribution and can be expressed as follows:

$$R(d_u) = R_3 + d_1 e^{-d_2 d_u}, \tag{7}$$

$$R(d_r) = \frac{1}{2} R_3 + d_1 e^{-d_2 d_r}. \tag{8}$$

In Eqs. (7) and (8), R_3 is an initial value. Moreover, d_2 is related to r, s, Δ, D, and θ. According to Fig. 5(c), the random depression has a half of the initial incident value of the uniform depression. Both of them have an exponential tendency. When the depression degree $d = 0\%$–100%, the variety of reflectance for the uniform depression is 15%, while it is less than 4% for the random depression.

5. CONCLUSION

In summary, for the first time, we have achieved a quantitative relationship between reflectance and nanosphere radius, incident light wavelength, polarization state, oxide material, and surface depression by an oxide nanosphere model. By adjusting the radius of the nanospheres, the reflectance can be reduced by up to 66% compared to the uncoated glass for the incident light of 550 nm with 75° incident angle. According to this model, the 80 nm nanosphere layer has a maximum reflectance of 3% at a normal incident wavelength of 480 nm, which is comparable to the previous report [29]. When the incident angle $\theta \leq 30°$, the reflectance of the nanosphere film can be quickly estimated by the effective refractive index. Our work will have potential applications in various fields [30–33], especially in transparent optics like high-digital screens and lenses. The model and laws of this study can be generalized not only in ultraviolet but also in infrared bands.

Funding. Scientific Research Fund of Sichuan Provincial Education Department (17CZ0038).

REFERENCES

1. P. Spinelli, M. Verschuuren, and A. Polman, "Broadband omnidirectional antireflection coating based on subwavelength surface Mie resonators," Nat. Commun. **3**, 692 (2012).

2. K. Im, J.-H. Kang, and Q.-H. Park, "Universal impedance matching and the perfect transmission of white light," Nat. Photonics **12**, 143–149 (2018).
3. P. Clapham and M. Hutley, "Reduction of lens reflexion by the "Moth Eye" principle," Nature **244**, 281–282 (1973).
4. Y. Li, J. Zhang, and B. Yang, "Antireflective surfaces based on biomimetic nanopillared arrays," Nano Today **5**, 117–127 (2010).
5. Z. Yu, H. Gao, W. Wu, H. Ge, and S. Y. Chou, "Fabrication of large area subwavelength antireflection structures on Si using trilayer resist nanoimprint lithography and liftoff," J. Vac. Sci. Technol. B **21**, 2874–2877 (2003).
6. X. Ye, J. Huang, F. Geng, H. Liu, L. Sun, L. Yan, X. Jiang, W. Wu, and W. Zheng, "High power laser antireflection subwavelength grating on fused silica by colloidal lithography," J. Phys. D **49**, 265104 (2016).
7. S.-S. Lo, C.-C. Chen, F. Garwe, and T. Pertch, "Broad-band antireflection coupler for a: Si thin-film solar cell," J. Phys. D **40**, 754–758 (2007).
8. E. Garnett and P. Yang, "Light trapping in silicon nanowire solar cells," Nano Lett. **10**, 1082–1087 (2010).
9. S. Jeong, M. D. McGehee, and Y. Cui, "All-back-contact ultra-thin silicon nanocone solar cells with 13.7% power conversion efficiency," Nat. Commun. **4**, 2950 (2013).
10. Z. Fan, R. Kapadia, P. W. Leu, X. Zhang, Y.-L. Chueh, K. Takei, K. Yu, A. Jamshidi, A. A. Rathore, and D. J. Ruebusch, "Ordered arrays of dual-diameter nanopillars for maximized optical absorption," Nano Lett. **10**, 3823–3827 (2010).
11. M. Grzelczak, J. Vermant, E. M. Furst, and L. M. Liz-Marzan, "Directed self-assembly of nanoparticles," ACS Nano **4**, 3591–3605 (2010).
12. Y. Kanamori, M. Sasaki, and K. Hane, "Broadband antireflection gratings fabricated upon silicon substrates," Opt. Lett. **24**, 1422–1424 (1999).
13. Y. Zhao, J. Wang, and G. Mao, "Colloidal subwavelength nanostructures for antireflection optical coatings," Opt. Lett. **30**, 1885–1887 (2005).
14. F. Tao, P. Hiralal, L. Ren, Y. Wang, Q. Dai, G. A. Amaratunga, and H. Zhou, "Tuning the peak position of subwavelength silica nanosphere broadband antireflection coatings," Nanoscale Res. Lett. **9**, 361 (2014).
15. R. Prado, G. Beobide, A. Marcaide, J. Goikoetxea, and A. Aranzabe, "Development of multifunctional sol-gel coatings: Anti-reflection coatings with enhanced self-cleaning capacity," Sol. Energy Mater. Sol. Cells **94**, 1081–1088 (2010).
16. J.-H. You, B.-I. Lee, J. Lee, H. Kim, and S.-H. Byeon, "Superhydrophilic and antireflective $La(OH)_3/SiO_2$-nanorod/nanosphere films," J. Colloid. Interface Sci. **354**, 373–379 (2011).
17. C.-C. Hsu, W.-L. Lan, N.-P. Chen, and C.-C. Wu, "The hydrophobic and omnidirectional antireflection coating of SiO_2 nanospheres with C_{18}-TEOS," Opt. Laser. Technol. **58**, 202–206 (2014).
18. X. Du and J. He, "Facile fabrication of hollow mesoporous silica nanospheres for superhydrophilic and visible/near-IR antireflection coatings," Chemistry **17**, 8165–8174 (2011).
19. J. Grandidier, M. G. Deceglie, D. M. Callahan, and H. A. Atwater, "Simulations of solar cell absorption enhancement using resonant modes of a nanosphere array," J. Photonics Energy **2**, 024502 (2012).
20. C. Atkinson, C. L. Sansom, H. J. Almond, and C. P. Shaw, "Coatings for concentrating solar systems-A review," Renew. Sustain. Energy Rev. **45**, 113–122 (2015).
21. A. Grosjean, A. Soum-Glaude, P. Neveu, and L. Thomas, "Comprehensive simulation and optimization of porous SiO_2 antireflective coating to improve glass solar transmittance for solar energy applications," Sol. Energy. Mater. Sol. Cells **182**, 166–177 (2018).
22. B. Xia, J. Luo, Y. Li, B. Yang, and S. Zhang, "Preparation of sponge-like porous SiO_2 antireflective coatings with excellent environment-resistance by an acid-catalysed sol-gel method," RSC Adv. **7**, 26834–26838 (2017).
23. C.-N. Chen, M.-J. Wu, C.-F. Hsu, and J.-J. Huang, "Antireflection coating of SiO_2 thin film in dye-sensitized solar cell prepared by liquid phase deposition," Surf. Coat. Technol. **320**, 28–33 (2017).
24. H. K. Raut, V. A. Ganesh, A. S. Nair, and S. Ramakrishna, "Anti-reflective coatings: A critical, in-depth review," Energy Environ. Sci. **4**, 3779–3804 (2011).
25. J. S. Metzman, G. Wang, J. R. Morris, and J. R. Heflin, "Enhanced scratch resistance of self-assembled silica nanoparticle anti-reflection coatings," J. Mater. Chem. C **6**, 823–835 (2018).
26. R. D. Shannon, R. C. Shannon, O. Medenbach, and R. X. Fischer, "Refractive index and dispersion of fluorides and oxides," J. Phys. Chem. Ref. Data. **31**, 931–970 (2002).
27. China's aladdin Chemical Company, http://www.aladdin-e.com/zh_cn/.
28. W. Luk, K. Yeung, K. Tam, K. Ng, K. Kwok, C. Kwong, A. Ng, and A. Djurišić, "Enhanced conversion efficiency of polymeric photovoltaic cell by nanostructured antireflection coating," Org. Electron. **12**, 557–561 (2011).
29. Y.-F. Huang, S. Chattopadhyay, Y.-J. Jen, C.-Y. Peng, T.-A. Liu, Y.-K. Hsu, C.-L. Pan, H.-C. Lo, C.-H. Hsu, and Y.-H. Chang, "Improved broadband and quasi-omnidirectional anti-reflection properties with biomimetic silicon nanostructures," Nat. Nanotechnol. **2**, 770–774 (2007).
30. J. Liu, F. Fan, Z. Feng, L. Zhang, S. Bai, Q. Yang, and C. Li, "From hollow nanosphere to hollow microsphere: mild buffer provides easy access to tunable silica structure," J. Phys. Chem. C **112**, 16445–16451 (2008).
31. S. Yancey, W. Zhong, J. R. Heflin, and A. L. Ritter, "The influence of void space on antireflection coatings of silica nanoparticle self-assembled films," J. Appl. Phys. **99**, 034313 (2006).
32. G. San Vicente, R. Bayón, N. Germán, and A. Morales, "Long-term durability of sol-gel porous coatings for solar glass covers," Thin Solid Films **517**, 3157–3160 (2009).
33. P. Buskens, M. Burghoorn, M. C. D. Mourad, and Z. Vroon, "Antireflective coatings for glass and transparent polymers," Langmuir **32**, 6781–6793 (2016).